Research Square

Preprints are preliminary reports that have not undergone peer review.
They should not be considered conclusive, used to inform clinical practice,
or referenced by the media as validated information.

Imaging Anatomy and Surface Localization of External Control Device - Target ed Arteries for Noncompressible Torso Hemorrhage

huayu zhang
Army Medical University
yong guo
Army Medical University
heng liu
Army Medical University
hao tang
Army Medical University
yang li
Army Medical University
lianyang zhang (dpzhangly@163.com)
Army Medical University https://orcid.org/0000-0002-4882-7280

Research article

Keywords: noncompressible torso hemorrhage, external hemorrhage control devices, surface landmark, imaging anatomy, 3D printing

Posted Date: December 10th, 2020

DOI: https://doi.org/10.21203/rs.3.rs-122489/v1

License: This work is licensed under a Creative Commons Attribution 4.0 International License.
Read Full License

Abstract

Background: Noncompressible torso hemorrhage (NCTH) is the main cause of prehospital death due to war injury. External hemorrhage control devices (EHCDs) are effective in reducing the death risk of NCTH, but the pressurized area is too large to prevent serious organ damage. This study aims to establish the surface localization strategy of EHCDs based on anatomical features of NCTH-related arteries through human CT images to facilitate the optimal design and application of EHCDs and eventually reduce relevant injuries.

Methods: Images of 200 patients aged 18-65 years who underwent abdominal contrast-enhanced CT scans were collected. Anatomical parameters such as the length and diameter of the aortic bifurcation (AB), common iliac artery (CIA), external iliac artery (EIA) and common femoral artery (CFA) were measured, and positional relationships among EHCD-targeted arteries, umbilicus, anterior superior iliac spine (ASIS) and pubic tubercle (PT) were determined. The accuracy of surface localization was verified by 3D-printed mannequins of 20 real patients.

Results: The angle and diameter of the AB were 47.1±10.5° and 17.8±2.7 mm, respectively. The AB was 7.5±8.6 mm to the left of umbilicus. The left CIA and right EIA were longer than the contralateral CIA and right EIA (p=0.038 and p=0.000, respectively). The average length of CFA was 39.0±16.6 mm. The CIA was wider than the EIA and the CFA (p=0.000). The distance between the artery and surface decreased from the CIA to the CFA (p=0.000). The vertical distance between the CIA terminus and the ipsilateral AB-ASIS line was 19.6±8.2 mm, and the left and right perpendicular intersections were located at the upper 1/3 and 1/4 of the AB-ASIS line, respectively. The length ratio of EIA-ASIS to ASIS-PT was 0.6:1. The length of the surface location/actual subpoint-ASIS was significantly correlated ($p \leq 0.002$), and the vertical distance between the two points of the same artery was ≤ 5.5 mm.

Conclusion: The arterial localization strategy established via anatomical investigation was consistent with the actual situation. The data are necessary for improving EHCD design, precise hemostasis and EHCD-related collateral injuries.

Introduction:

Records of the U.S. Army's operations in the 21st century have shown that nearly 90% of the deaths tragically occurred in prehospital scenarios, and 80% of the potentially survivable deaths (PSs) were hemorrhage-related. The abdomen, pelvic cavity and groin, which consist of most of the torso and junctional regions, are extremely vulnerable, and conventional limb tourniquets are invalid(1, 2); thus, this type of hemorrhage is called NCTH(3).

The promotion of tourniquets for extremities by the guidelines of tactical combat casualty care (TCCC) was efficient, which significantly reduced the mortality rate of limb bleeding by 85% (4). Similarly, to reduce the death risk at the scene of injury or in the process of evacuation, adding opportunities to receive

definitive treatment in medical treatment facilities (MTFs), Holcomb et al. called for an improvement of NCTH emergency control techniques to ameliorate the survival rate (5).

The emergence of EHCDs, such as combat ready clamp (CRoC), abdominal aortic and junctional tourniquet (AAJT) and SAM junctional tourniquet (SJT), has changed the dilemma of ineffective control of NCTH within battlefields or extreme environments, providing the possibility for further reducing the rate of killed in action (KIA)(6, 7). However, too broad of a pressurized area and ambiguous vascular locating methods are ubiquitous among existing EHCDs, often resulting in excessive peripheral tissue/organ compression or high compression segments of targeted arteries. The resultant ischemic/mechanical injuries and limb dysfunction obviously inhibit the promotion of EHCDs in clinical practice(8–10).

In contrast, benefiting from applied anatomy research of related arteries, in-hospital application of resuscitative endovascular balloon occlusion of the aorta (REBOA) has been developed rapidly by virtue of excellent hemostatic and resuscitative effects and the relatively controllable risk of complications (11, 12). With the continuous improvement of vascular surface localization strategies(13), REBOA catheterization relies less on image-assisted technology. Regrettably, due to the need for strict sterile techniques and its application by highly trained doctors only, it cannot be applied to NCTH prehospital salvation in the near future(14). EHCDs, however, as highly integrated and user-friendly equipment, are more advantageous than REBOA in the popularization of frontline operating forces and civilian emergency medical services (EMS).

As the ultimate challenge of war injuries, state-of-the-art hemostatic equipment and strategies are desperately needed for NCTH prehospital emergency assistance. Therefore, next-generation EHCDs should focus on optimizing the localization strategy to minimize the invasion of arteries, tissues and organs in nonoperating areas and eventually to realize the aim of precise external compression hemostasis.

The current study was dual-purpose directed. (A) The anatomical features of NCTH-related abdominal and pelvic arteries and their positional relationship with surface landmarks such as the umbilicus, ASIS, PT were determined via total abdominal contrast-enhanced CT imaging. (B) The accuracy of arterial body surface localization was verified on 3D-printed full-size dummies using data collected from real patients.

Materials And Methods:

(A) The anatomic features of EHCD-targeted arteries and their positional relationship with surface landmarks

Inclusion criteria: Original imaging data and demographic information of 200 consecutive Chinese patients aged between 18-65 years who underwent total abdominal contrast-enhanced CT scan in the imaging center of a tertiary hospital where the researchers worked were collected.

Exclusion criteria: Spinal deformity (lordosis/kyphosis/scoliosis), spinal tumor, abdominal aortic aneurysm, obvious dilation or tortuosity of main arteries, space-occupying lesion or visceromegaly leading to vascular deviation from anatomical position, and difficulty in film reading due to poor vascular imaging, artifact, foreign body or improper body position.

Imaging equipment and software: Images were acquired by a Light Speed VCT (GE MEDICAL SYSTEMS, USA) or a Philips Brilliance iCT 256 (Philips Health care, Netherlands) with a scanning thickness of 0.625 mm. The parameters were measured by Philips Intellispace Portal v6.0.5.02900 image processing software (Philips Health Care, Netherlands).

Parameters:

(1) Arteries: The distances from the AB to the main branches of the abdominal aorta (AA), such as the celiac trunk (CET), superior mesenteric artery (SMA), inferior mesenteric artery (IMA), and renal artery (RA) were measured. The length and inner diameter of the AB, CIA, EIA and CFA were determined (the ASIS-PT line was substituted for the inguinal ligament due to the poor image development of the latter, and the intersection of the EIA and the ASIS-PT was regarded as the origin of the CFA). The positional relationships among the AB, umbilical subpoint, CFA terminus, vertebrae, ASIS and femoral head were determined by transverse, sagittal and coronal planes. The vertebrae were equally divided into 3 segments horizontally and vertically (Figure 1A), while the femoral head was divided into five parts along the trunk axis (Figure 1B). Vascular length, diameter, angle and vertical distance between planes were measured by coronal volume render (VR) imaging (Figure 1C). The vertical distance from the arterial anterior wall to the body surface was determined via transverse imaging (Figure 1D).

(2) Surface landmarks: The distances between ASISs, length of AB-ASIS line and vertical distance of umbilical-AB were measured. The distances and positions among the ASIS, umbilical subpoint, AB, CIA or EIA were also determined (Figure 1E, 1F).

(B) Image reconstruction and full-size dummy 3D printing and verification of arterial body surface localization

(1) 3D printing: Enhanced CT images of 20 patients (10 for each sex) with normal body mass index (BMI) and arterial morphology were selected. During image reconstruction, projection points of the AB, CIA/EIA/CFA terminus, ASIS and PT were identified (Figure 2A), and a 1.0-mm-diameter hole in the corresponding position of the abdominal wall was formed during printing to facilitate comparison with the surface localization strategy. The aperture was too small to be discovered without added light; thus, it would not interfere with the research process. The dummy was constituted by a chest and abdominal wall, AA and main branches, CIA, EIA, CFA, spine and pelvic ring (Figure 2B, 2C).

(2) Verification of the arterial body surface localization: First, researcher A measured the length of the AB-left ASIS and the distance from the CIA/EIA/CFA terminus to the ipsilateral ASIS on the model's body surface using a divider (Figure 2D). Then, the positions of the ASIS and PT were marked with a red marking pen to facilitate localization with surface landmarks. Third, researcher B, who was single-blinded to the study, was guided to localize the above arteries based on the surface localization strategy with a black marking pen. Finally, researcher A measured the distance from the black marks to the corresponding ASIS and the transverse/longitudinal vertical distance between the actual projection point of each artery and the corresponding black point.

Statistical analysis:

The data were analyzed by SPSS 25.0 (SPSS, Chicago, USA). Mean ± SD was used to calculate continuous variables. Student`s *t* test and one-way ANOVA were used for comparisons among groups, and Pearson's test was used for correlation analysis. A Bland-Altman graph was generated by MedCalc 15.8 (MedCalc Software, Ostend, Belgium) to compare the difference between body surface localization and the actual projection point of the same artery. $p<0.05$ was considered statistically significant.

Ethics approval and consent to participate:

This study was approved by the Ethics Committee of Daping Hospital (Army Medical Center of PLA) (reference number 2019092) and conducted in adherence with the tenets of the Declaration of Helsinki. Informed consent was waived because patients` private information were hided, and all data were not used for commercial or medical purposes.

Results:

1. Demographic information:

From July 13, 2020 to August 6, 2020, a total of 509 patients underwent whole-abdomen enhanced CT scanning. Two hundred (39.3%) patients with an average age of 42.7 ± 12.8 years met the inclusion criteria, among whom females accounted for 47.5% (Table 1). The average BMI was 22.6 ± 3.7, 23 cases (11.5%) had BMIs of less than 18.5, and 26% were considered overweight (BMI ≥ 25). Among 309 (60.7%) excluded cases, 58.6% were excluded for improper age, 37.9% due to poor arterial morphology, and the remaining 11 cases for improper body position or presence of a foreign body.

Table 1
Demographic information of included cases

	Total (n, %)	Male (n, %)	Female (n, %)	*p*
Number	200, 100.0%	105, 52.5%	95, 47.5%	/
Age (years)	42.7 ± 12.8	40.0 ± 12.6	45.7 ± 12.3	0.001
BMI	22.6 ± 3.7	23.1 ± 3.9	22.0 ± 3.3	0.044
BMI: body mass index				

2. AA:

2.1 Main branches of the AA:

The distance from the AB to the superior border of the CET or the inferior border of the SMA/the lowest RA/IMA was 131.1 ± 11.8 mm, 112.5 ± 10.7 mm, 94.7 ± 9.9 mm or 41.9 ± 8.3 mm. The superior border of the CET was 36.4 ± 8.1 mm from the lowest RA. The CET mainly originated at the lower left 1/3 (57.1%) of T12 (42.0%), ranging from the T11-12 intervertebral disc to the upper 1/3 of L1. The origin of the SMA was at the lower left 1/3 (23.4%) of L1 (68.5%), ranging from the T12-L1 intervertebral disc to the upper 1/3 of L2. The IMA often started from the lower median 1/3 (31.4%) of L3 (70.0%), ranging from the L2-3 intervertebral disc to the median 1/3 of L4. The left RA was located at the lower left 1/3 (48.6%) of L1 (36.0%), ranging from the T12-L1 intervertebral disc to the lower 1/3 of L2. The left RA was lower than the opposite side in 72.5% of patients, and the latter commonly started at the lower median 1/3 (53.8%) of L1 (46.5%), ranging from the intervertebral discs between T12-L1 and L2-3.

2.2 AB:

The vertical distance from the AB to the abdominal wall was 82.4 ± 28.4 mm, the width of the bifurcation was 17.8 ± 2.7 mm, and the diameter 10 mm above the AB was 13.5 ± 1.8 mm. The angle of the AB was 47.1 ± 10.5°. It was commonly located at the lower median 1/3 (41.4%) of L4 (64.0%), ranging from the lower 1/3 of L3 to the median 1/3 of L5. The length of the ASIS on both sides was 229.2 ± 16.8 mm, the AB was 91.7 ± 14.9 mm from the midpoint of this virtual line, and the vertical distance between the AB and the ASIS line was 91.3 ± 14.9 mm. The AA (85.5%) was mainly located on the left side, 7.0 ± 5.1 mm from the center, if the torso was equally divided into two halves by the midpoint of the ASIS line. Meanwhile, the AB-right ASIS line was longer than the AB-left ASIS line (151.2 ± 13.5 mm vs. 142.5 ± 12.9 mm, $p = 0.000$). Similarly, the umbilicus was also commonly located at the lower median 1/3 (29.5%) of L4 (64.5%), ranging from the median 1/3 of L3 to the lower 1/3 of L5 (Fig. 3). The vertical depth from the umbilicus to the AB was 72.8 ± 26.3 mm. Taking the AB as the origin of coordinates, the longitudinal and transverse vertical distances between the AB-umbilicus subpoints were 0.3 ± 14.7 mm and − 7.5 ± 8.6 mm, respectively (Fig. 4).

3. CIA, EIA and CFA:

3.1 Numerical parameters:

The left CIA was slightly longer than the contralateral (46.6 ± 16.0 mm vs. 43.3 ± 15.5 mm, p = 0.038), and the angle between the former and the AA was also broader than that of the latter (158.1 ± 9.1 mm vs. 156.5 ± 7.6 mm, $p = 0.047$). The left CIA terminus was often lower than the opposite (63.5), and the longitudinal vertical distance between them was 8.9 ± 6.6 mm. The right EIA was longer than the opposite side (111.5 ± 18.8 mm vs. 102.6 ± 16.3 mm, $p = 0.000$), while no significant difference was detected between bilateral CFAs (37.7 ± 16.0 mm vs. 40.3 ± 17.2 mm, $p = 0.120$). Notably, the straight distance between the origin and terminus of the CIA, EIA or CFA was not significantly different from the actual length of the corresponding artery. The diameters of the CIA, CFA and EIA midpoints gradually decreased (7.6 ± 1.4 mm vs. 6.4 ± 1.3 mm vs. 5.1 ± 1.2 mm, $p = 0.000$), and only the diameter of the CIA showed a statistically bilateral difference (left: 7.5 ± 1.4 mm vs. right: 7.8 ± 1.4 mm, $p = 0.025$).

3.2 Positional relationship:

The vertical length between the left CIA terminus and the AB-homolateral ASIS line was 20.4 ± 7.8 mm, and the contralateral length was 18.8 ± 8.5 mm ($p = 0.041$). The distance between the left intersection of the above perpendicular and homolateral ASIS was shorter than the opposite (100.7 ± 15.3 mm vs. 112.0 ± 17.4 mm, $p = 0.000$). Both the distances of the left/right EIA terminus to the homolateral ASIS (left: 65.1 ± 8.0 mm vs. 65.5 ± 8.4 mm, $p = 0.611$) and the ASIS-homolateral PT line (left: 115.1 ± 9.1 mm vs. right: 115.2 ± 8.6 mm, $p = 0.843$) showed no significant differences. The left CIA midpoint was closer to the surface than the opposite (86.3 ± 26.0 mm vs. 80.9 ± 26.8 mm, $p = 0.042$), and the vertical distance from the arterial midpoint to the body surface gradually decreased from the CIA to the CFA (83.6 ± 26.5 mm vs. 68.8 ± 24.5 mm vs. 23.4 ± 11.2 mm, $p = 0.000$). Both CFA termini were commonly located beneath the femoral head (left: 52.5%, right: 60.0%).

4. Effects of gender, age and BMI on anatomical parameters:

AB (female: 30.5%, male: 22.9%) and umbilical subpoints (female: 66.3%, male: 70.5%) were commonly located in the lower median 1/3 of L4 for both genders. The distances of CET-AB, SMA-AB and lowest RA-AB of females were all shorter ($p = 0.000$). Meanwhile, some structures related to EHCDs had significant gender differences as well as age and BMI correlations (Tables 2 and 3).

Table 2
Gender differences in EHCD-related structures

	Male	Female	*p*
Angle of AB	48.7 ± 9.6	45.6 ± 11.2	0.041
Vertical distance of the AB-bilateral ASIS line	94.2 ± 16.3	88.7 ± 13.0	0.010
Distance of the AB-EIA terminus	152.6 ± 15.4	146.7 ± 15.3	0.000
Length of the EIA	109.2 ± 18.7	105.0 ± 17.4	0.020
Vertical distance of the CIA midpoint-body surface	79.0 ± 24.1	87.7 ± 27.9	0.001
Vertical distance of the EIA midpoint-body surface	72.3 ± 23.9	65.6 ± 24.7	0.006
Distance of the ASIS-PT	113.3 ± 8.9	116.9 ± 8.4	0.000
Vertical distance between the CIA terminus and the AB-ASIS line	18.3 ± 7.7	20.7 ± 8.4	0.003
Distance of the CFA origin-ASIS	63.2 ± 7.4	67.3 ± 8.4	0.000
Length of the CFA	32.0 ± 14.8	45.3 ± 15.6	0.000
Diameter 10 mm above the AB	12.8 ± 1.7	14.2 ± 1.7	0.000
Width of the AB	17.1 ± 2.6	18.4 ± 2.7	0.001
Diameter of the CIA midpoint	7.2 ± 1.3	8.0 ± 1.4	0.000
Diameter of the EIA midpoint	4.6 ± 0.9	5.6 ± 1.3	0.000
Diameter of the CFA midpoint	6.0 ± 1.1	6.8 ± 1.2	0.000
Vertical distance of the umbilicus-AB	66.9 ± 24.4	78.2 ± 27.0	0.002
Longitudinal distance of the umbilicus subpoint-AB	-3.8 ± 15.7	3.9 ± 12.7	0.000
Vertical distance of the AB-body surface	75.9 ± 25.3	88.2 ± 29.9	0.002

EHCDs: external hemorrhage control devices, AB: aortic bifurcation, ASIS: anterior superior iliac spine, PT: pubic tubercle, CIA: common iliac artery, EIA: external iliac artery, CFA: common femoral artery. mm for length and diameter, ° for angle

Table 3
Correlation analysis of EHCD-related structures with age and BMI

	Age	BMI
Angle of the AB	r = 0.109, *p* = 0.124	r=-0.245, p = 0.000
Vertical distance of the AB-bilateral ASIS line	r=-0.140, p = 0.047	r = 0.076, *p* = 0.288
Vertical distance between the CIA terminus and the AB-ASIS line	r=-0.130, p = 0.009	r = 0.049, *p* = 0.330
Distance of the EIA terminus-ASIS	r=-0.323, p = 0.000	r=-0.065, *p* = 0.197
Distance of the AB-EIA terminus	r=-0.234, p = 0.000	r = 0.003, *p* = 0.947
Vertical distance of the umbilicus-AB	r = 0.161, p = 0.022	r = 0.597, p = 0.000
Vertical distance of the AB-body surface	r = 0.125, *p* = 0.077	r = 0.614, p = 0.000
Longitudinal distance of the umbilicus subpoint-AB	r=-0.004, *p* = 0.951	r=-0.152, p = 0.031
Vertical distance of the CIA midpoint-body surface	r = 0.172, p = 0.001	r = 0.624, p = 0.000
Vertical distance of the EIA midpoint-body surface	r = 0.435, p = 0.000	r = 0.501, p = 0.000
Vertical distance of the CFA midpoint-body surface	r = 0.220, p = 0.000	r = 0.614, p = 0.000
Diameter 10 mm above the AB	r = 0.148, p = 0.036	r = 0.290, p = 0.000
Width of the AB	r = 0.275, p = 0.000	r = 0.324, p = 0.000
Diameter of the CIA midpoint	r = 0.120, p = 0.017	r = 0.232, p = 0.000
Diameter of the EIA midpoint	r=-0.035, *p* = 0.485	r = 0.306, p = 0.000
Diameter of the CFA midpoint	r = 0.062, *p* = 0.214	r = 0.154, p = 0.002

EHCDs: external hemorrhage control devices, BMI: body mass index, AB: aortic bifurcation, ASIS: anterior superior iliac spine, PT: pubic tubercle, CIA: common iliac artery, EIA: external iliac artery, CFA: common femoral artery. mm for length and diameter, ° for angle

The patients were further divided into 4 groups according to their age. The width of the AB and the vertical distance of the EIA/CFA midpoint-body surface were positively correlated with age, while the vertical distance between the CIA terminus and the AB-ASIS and the length of the EIA terminus-ASIS showed a negative trend (Table 4).

Table 4
Anatomical differences in EHCD-related structures with age

	Group 1: 18–29 (n, %)	Group 2: 30–41 (n, %)	Group 3: 42–53 (n, %)	Group 4: 54–65 (n, %)	Differences among groups (*p*)
Number	43, 21.5%	45, 22.5%	67, 33.5%	45, 22.5%	/
BMI	21.6 ± 4.2	22.4 ± 3.8	23.0 ± 3.0	23.1 ± 3.7	0.173
Width of the AB	16.7 ± 2.3	17.4 ± 2.0	18.3 ± 3.1	17.8 ± 2.7	0.003
Vertical distance between the CIA terminus and the AB-ASIS	21.7 ± 9.3	19.8 ± 7.5	18.8 ± 8.1	18.5 ± 7.4	0.041
Distance of the EIA terminus-ASIS	69.6 ± 9.3	66.5 ± 7.2	63.4 ± 7.3	63.0 ± 7.5	0.000
Vertical distance of the EIA midpoint-body surface	52.7 ± 18.5	62.0 ± 20.4	74.7 ± 22.0	81.9 ± 26.6	0.000
Vertical distance of the CFA midpoint-body surface	19.8 ± 9.9	22.1 ± 10.7	24.1 ± 9.3	27.0 ± 13.9	0.00

EHCDs: external hemorrhage control devices, BMI: body mass index, AB: aortic bifurcation, ASIS: anterior superior iliac spine, PT: pubic tubercle, EIA: external iliac artery, CFA: common femoral artery. mm for length

Among patients with different BMIs, the larger the BMI, the smaller the angle of the AB, and the longer the vertical distance of the umbilicus-AB. Otherwise, arterial diameter and the vertical distance of the arterial wall surface showed roughly positive correlations with BMI (Table 5).

Table 5
Anatomical differences in EHCD-related structures with BMI

	Group 1: <18.5 (n, %)	Group 2: 18.5–24.9 (n, %)	Group 3: ≥25 (n, %)	Differences among groups (*p*)
Number	23, 11.5%	125, 62.5%	52, 26.0%	/
Age	35.6 ± 14.3	43.3 ± 12.2	44.4 ± 12.7	0.015
Angle of the AB	52.5 ± 9.4	47.4 ± 9.9	43.8 ± 11.5	0.003
Diameter 10 mm above the AB	12.5 ± 1.7	13.5 ± 1.7	14.2 ± 2.0	0.001
Width of the AB	16.1 ± 2.4	17.8 ± 2.4	18.6 ± 3.3	0.001
Diameter of the CIA midpoint	6.9 ± 1.6	7.6 ± 1.3	8.0 ± 1.5	0.000
Diameter of the EIA midpoint	4.4 ± 0.9	5.0 ± 1.2	5.5 ± 1.2	0.000
Diameter of the CFA midpoint	5.8 ± 1.2	6.5 ± 1.3	6.6 ± 1.1	0.002
Vertical distance of the umbilicus-AB	51.6 ± 20.0	68.1 ± 22.4	93.6 ± 24.7	0.000
Vertical distance of the AB-body surface	58.4 ± 20.6	77.2 ± 24.0	105.3 ± 26.5	0.000
Vertical distance of the CIA midpoint-body surface	60.4 ± 18.8	79.2 ± 22.6	104.4 ± 24.6	0.000
Vertical distance of the EIA midpoint-body surface	47.2 ± 20.8	66.7 ± 22.0	83.2 ± 23.3	0.000
Vertical distance of the CFA midpoint-body surface	13.0 ± 8.0	21.6 ± 8.8	32.2 ± 11.6	0.000

EHCDs: external hemorrhage control devices, BMI: body mass index, AB: aortic bifurcation, CIA: common iliac artery, EIA: external iliac artery, CFA: common femoral artery. mm for length and diameter, ° for angle

5. Verification of body surface localization strategy:

Full-size 3D-printed dummies were printed according to the images of 20 patients (Table 6).

Table 6
Demographic information of 3D-printed models

	Total (n, %)	Female (n, %)	Male (n, %)	*p*
Number	20, 100.0%	10, 50.0%	10, 50.0%	/
Age	26.4 ± 5.5	25.4 ± 4.1	27.4 ± 6.8	0.435
BMI	21.3 ± 1.7	20.9 ± 1.8	21.7 ± 1.5	0.302
BMI: body mass index				

The horizontal perpendicular length of the umbilical subpoint-AB was roughly the width of the little finger in both genders (female: -7.3 ± 8.9 mm vs. male: -7.7 ± 8.3 mm, $p = 0.728$), and the longitudinal distance of the umbilicus subpoint-AB was less than 5 mm (female: -3.8 ± 15.7 mm, male: 3.9 ± 12.7 mm); hence the AB and the umbilicus were located at approximately the same horizontal plane. Due to the close positional relationship between the AB and the umbilicus, investigators chose to replace the AB with the umbilicus, which was more intuitive when the CIA terminus was localized via the surface landmark method. The perpendicular length between the CIA termini and the homolateral AB-ASIS was approximately the width of the thumb (left, female: 19.3 ± 7.3 mm vs. male: 21.4 ± 8.0 mm, $p = 0.049$; right, female: 17.4 ± 8.0 mm vs. male: 20.0 ± 8.8 mm, $p = 0.027$). No significant difference was observed in the distance (L_1) of the umbilicus-left/right ASIS and the length (L_2) between the intersection of the homolateral CIA terminus with the line mentioned above and the ASIS; the ratios of L_1 to L_2 on left/right side were 70.8% and 74.1%, respectively, approximately equal to 2/3 and 3/4. Similarly, there was no significant difference within each gender in the length (L_3) of inguinal ligaments and the length of the EIA terminus-ipsilateral ASIS, L_4:L_3 = 55.8%-57.8%, roughly equal to 3/5 the length of inguinal ligament. The CIA, EIA and CFA were straightly downward from their origins, verified by the lack of significant difference between the distance of the arterial origin-terminus and the actual length of the same artery. There was no difference in the female CFA length on either side (31.6 ± 13.8 mm vs. 32.4 ± 15.8 mm, $p = 0.727$); therefore, the CFA terminus was approximately 2 finger breadths away from its origin. Tiny directional differences existed in the male CFA length (43.2 ± 15.9 mm vs. 47.4 ± 15.1 mm, $p = 0.049$), and the CFA terminus could be found 3 fingers below the origin (Table 7, Fig. 5).

Table 7
Surface localization of EHCD-related arteries

	Surface landmark	Localization strategy
AB	Umbilicus	1 fingerbreadth (little finger) to the left of the umbilicus
Left CIA terminus	Umbilicus-ASIS	Upper 1/3 of the line, then parallelly downward by 1 finger-breadth (thumb)
Right CIA terminus	Umbilicus-ASIS	Upper 1/4 of the line, then parallelly downward by 1 finger-breadth (thumb)
EIA termini	ASIS-PT	Inner 2/5 of the line
CFA termini	ASIS-PT	Female: inner 2/5 of the line, then vertically downward by 2 finger-breadths Male: inner 2/5 of the line, then vertically downward by 3 finger-breadths

EHCDs: external hemorrhage control devices, AB: aortic bifurcation, ASIS: anterior superior iliac spine, PT: pubic tubercle, CIA: common iliac artery, EIA: external iliac artery, CFA: common femoral artery

The distance of the AB-left ASIS and 1 finger-breadth left to the umbilicus-left ASIS and the length of the CIA/EIA/CFA terminus-ASIS and the actual arterial projection point-corresponding ASIS were statistically correlated; the absolute values of the mean horizontal and the longitudinal vertical distances of each actual arterial subpoint (AAS)-surface location (SL) were less than 5.5 mm and 4.2 mm, respectively (Table 8).

Table 8
Correlation analysis of the AAS and the corresponding SL

	Pearson correlation	Horizontal vertical distance of the AAS-SL*	Longitudinal vertical distance of the AAS-SL*
AB	r = 0.654, *p* = 0.002	3.5 ± 7.5	4.2 ± 12.1
Left CIA terminus	r = 0.856, *p* = 0.000	-1.1 ± 6.8	2.7 ± 14.8
Right CIA terminus	r = 0.652, *p* = 0.002	1.5 ± 6.2	2.8 ± 12.5
Left EIA terminus	r = 0.823, *p* = 0.000	-1.4 ± 3.0	-0.6 ± 2.7
Right EIA terminus	r = 0.861, *p* = 0.000	1.0 ± 4.1	-1.5 ± 3.3
Left CFA terminus	r = 0.686, *p* = 0.001	-5.5 ± 7.2	2.7 ± 9.0
Right CFA terminus	r = 0.794, *p* = 0.000	2.3 ± 5.9	0.6 ± 7.7

*: Taking the actual arterial subpoint as the datum point, a positive distance value occurred when the surface localization was situated on its left or above. AAS: actual arterial subpoint, SL: surface location, AB: aortic bifurcation, CIA: common iliac artery, EIA: external iliac artery, CFA: common femoral artery, mm for distance

Discussion:

The current study specified the lengths of REBOA-related Zone II (36.4 ± 8.1 mm) and Zone III (94.7 ± 9.9 mm), which were similar to those in previous studies (13, 15, 16). The CFA terminus of both sides was commonly located beneath the femoral head, which was consistent with Garrett's report(17). Despite exhaustive anatomical studies of REBOA, parameters related to the Chinese population are first revealed, which is important for enriching the ethnic database and guiding endovascular treatments involving Chinese patients.

This research focuses on a series of details highly related to the application and redesign of EHCDs. Therefore, it can be reasonably deemed the first applied anatomical study of EHCD-related arteries as well as the first surface localization strategy for external NCTH control.

1. The umbilicus is a reliable surface landmark for the AB. Gender, age and BMI can affect their positional relationship

The AB and umbilical subpoints are mainly located at the lower median 1/3 of L4, and the AB is nearly 10 mm left to the latter, which is similar to the literature(18–21) but higher than L5, as reported by Pirró(22). The angle of the AB in this study (47.1 ± 10.5°) was slightly smaller than measurements from cadavers (54 ± 16°)(23). Vascular deformation caused by aging, embalmment and intravascular fillings may account for the discrepancy(24). In addition, a negative correlation between BMI and the AB angle was found in this study (r=-0.245, $p = 0.000$), and the possibility that different body shapes among living patients and cadavers may affect the results should also be considered.

A series of studies have confirmed that the umbilicus is a reliable surface landmark for the AB(25–29), though the study populations were predominantly female(25–27, 29). The current study found that the vertical distance of the umbilicus-AB in women or skinny patients was smaller than that in men or obese people. It is rational to decrease the compression strength for the former when the umbilicus is used as the landing point of EHCDs to avoid extra damage. According to Attwell(28), the positional relationship of the AB and the umbilicus is not significantly correlated among patients aged under 65, but a positive correlation of the umbilicus-AB vertical distance was revealed by this study (r = 0.161, $p = 0.022$). Abdominal fat accumulation resulting from hypokinesia and metabolic dysfunction associated with aging may be the main cause for this phenomenon(30). However, aging is also naturally accompanied by decreases in abdominal muscle thickness and strength(31, 32); thus, age and body shape should only be used as a reference for predicting pressurization. The actual pressure and the end point of pressurization should still be determined by hemostasis or the pressure limit of EHCDs. A downward decreasing trend of the artery-surface distance is also detected. The relationship between the depth of arteries and pressurized degree has been preliminarily investigated in humans (34, 35).

The AB is the largest part among EHCD-related arteries, and the current result (17.8 ± 2.7 mm) lies between the previous data (14.0 mm-22.1 mm)(22, 33). Because the difference among CIA/EIA/CFA diameters is only a millimeter in magnitude, the author considers that a uniform size may be acceptable in designing pressurized components (PCs) for iliac and femoral arteries to reduce the time wasted by frequent PC replacement and resultant delays in hemostatic rescue.

Despite the close relationship among the AB, the umbilical subpoint and the L4 vertebra(20), a downward trend of AB position with aging and anatomical variation in the lumbosacral spine(21), the accuracy and clinical value of the L4 alone in localizing the AB declined. Hemostasis is a competition with time. The time to effective hemostasis will be undoubtedly extended by turning the wounded and counting the vertebrae for AB localization. In addition, it is difficult to turn over an individual when they are trapped in a narrow space, and rescuers may apply EHCDs only by their experience if no alternative localization method is available, thus increasing the risk of death from hemostatic failure. Therefore, anterior landmarks taken for artery localization are more intuitive and convenient.

2. The surface localization strategy is accurate to determine the position of EHCD-related arteries

Animal experiments have confirmed that EHCDs can cause serious organ damage with application times of as long as 4 hours(8). However, in extreme environments such as scenes of fierce fighting and austere situations or when transportation is damaged by earthquakes, the EHCD application time must be further extended, thus increasing the incidence and severity of subsequent ischemic damage. In addition, the existing EHCD applications heavily rely on clinical experience(36). Rough arterial localization may result in excessive pressurized areas or exceeding hemostatic segments, which thereby account for unnecessary peripheral tissue injuries. In contrast, the wounded may suffer a high incidence of prehospital death if medical workers try to minimize complications by reducing the application time. Redesign of EHCDs based on refinement of arterial targeted occlusion is helpful for disequilibrating the above balance.

Bland-Altman analysis evaluates the consistency of the new method with the “gold standard” by analyzing their difference value and LoA(37). The actual subpoint printed on the dummy surface is equal to the standard ultrasound localization method. Although the boundary of the LoA looks large, the AAS/SL-ASIS distance of the AB/CIA/EIA/CFA is commonly within ± 10 mm (75%-90%), the length between the AAS/SL of the EIA and the ASIS even fluctuates within ± 5 mm (left: 70%, right: 80%), and the relative distance error of the AAS/SL-ASIS is less than 9.1%. Combined with the average difference between AAS/SL-ASIS (ranging from − 0.1 mm-3.9 mm), data from this study suggest a promising potential surface localization strategy for NCTH external control. The depth of arteries and body surface morphology may intervene in the hemostatic effect. Thus, desired hemostasis is possibly achieved by the meticulous design of the PCs. The size of PCs may be several times the arterial diameter to maintain the balance of hemostasis and minimize organ damage. The vertical distance of the AAS-SL is no more than 4.1 mm, and such a tiny positional deviation is covered by the PCs. This conception can reduce the possibility of mispositioning and resultant hemostatic failure. Theoretically, the surface localization method offers an opportunity for refining NCTH control. The incidence and severity of EHCD-related damage can be reduced, a longer application time will be obtained, and eventually, the prehospital survival rate of NCTH will be improved. In addition, localization training is beneficial for understanding relevant anatomical knowledge and for improving the efficiency of prehospital first aid.

When applying EHCDs for shock patients resulting from blunt injury of the lower abdomen or pelvic fracture, the end of the AA or the AB is the acceptable landing point for PCs due to the unknown location of the damaged artery. However, given the significantly greater transverse diameter of the AB, the investigators suggest that 10 mm above the AB may be a better occlusion point for the purpose of rapid and definitive hemostasis. The scope and severity of ischemia will be limited when the pressurized segment approaches the bleeding artery(38). The confirmation of the location of the iliac and femoral artery termini is helpful to guide the appropriate pressuring site. When compressing the EIA, the occlusion position should be as close to the terminus as possible, but inguinal ligament coverage should be avoided. Similarly, the PC should be located close to or even partially across the CIA terminus when CIA compression is needed. When targeting the narrow inguinal region, pressure transmission will be disturbed because of mispositioning the PC onto the ligament. Genitalia compression may also lead to

disastrous outcomes. Therefore, distal and lateral PC placement should be attempted under the premise of effective hemostasis.

The PC is the key for the redesign of EHCDs. The main defect of existing EHCDs is the inability to precisely control the damaged arteries within the lower abdomen and relevant junctional regions(39). Based on the current study, the authors propose a proposal for EHCD improvement. The PCs are composed of 3 pressurized balloons and one spherical balloon 10 mm above the AB, and the size should be adequate for bleeding occlusion but not excessive to interrupt the lowest RA. The other two rectangle-like PCs target the CIA/EIA/CFA; the length can be designed based on the CFA length (the shortest distance), and the width is referred to by the CIA diameter (the widest distance). The optimal material and size need to be clarified in a follow-up study. The PC is fixed with a tourniquet by nylon stickers, and the position is flexible according to the shape of the body, the pressurized site and the targeted artery. The balloon is pumped independently to facilitate different pressure intensities for different arteries. The pumping starts from the lowest bleeding site; if the CFA or EIA bleeding is not well controlled, then the CIA or the end of the AA should be pressurized. Since the downstream blood flow has been partially controlled in advance, further restriction of upstream flow and velocity will result in acceptable hemostasis. Therefore, compared with occluding the AA alone, the novel strategy is expected to reduce the risk of extensive and severe EHCD-related ischemic injury. Relevant studies have been carried out in succession.

3. Limitations

There are several limitations in the current study. Patients older than 65 years were excluded from the analysis of anatomical parameters. Frontline forces are mainly constituted by young adults, and multiple epidemiologic studies have indicated that trauma is the leading cause of death among people under 65 who are prone to lose their lives before arriving at the MTF (40–42). Therefore, it is reasonable to believe that the included subjects have already covered the majority of people susceptible to traumatic hemorrhage. The first part of the study belongs to the category of observational research, and no intervention existed during recruitment. The differences in BMI and age between sexes not only reflect the nature of non-artificial data but also manifest the authenticity of the data. Due to the COVID-19 pandemic(43), researchers decided to replace volunteers with 3D-printed dummies to reduce person-to-person infection(44, 45). Since the data originated from live people, the printed models and relevant artery subpoints were qualified alternatives to “gold standard”-ultrasound vessel localization. In addition, the dummies can be repeatedly used in NCTH training, which is resource-friendly and beneficial in hemostatic training.

Conclusion:

Based on the analysis of anatomical parameters of NCTH-related arteries, this study determined the surface localization strategy of EHCDs, providing the necessary data for the development of precise

NCTH external control, broadening corresponding thoughts of clinical treatment and research and offering a new opportunity to further reduce prehospital mortality.

Abbreviations

NCTH: noncompressible torso hemorrhage; EHCDs: External hemorrhage control devices; AB: aortic bifurcation; CIA: common iliac artery; EIA: external iliac artery; CFA: common femoral artery; ASIS: anterior superior iliac spine; PT: pubic tubercle; PSs: potentially survivable deaths; TCCC: tactical combat casualty care; MTFs: medical treatment facilities; CRoC: combat ready clamp; AAJT: abdominal aortic and junctional tourniquet; SJT: SAM junctional tourniquet; KIA: killed in action; REBOA: resuscitative endovascular balloon occlusion of the aorta; EMS: emergency medical services; AA: abdominal aorta; CET: celiac trunk; SMA: superior mesenteric artery; IMA: inferior mesenteric artery; RA: renal artery; VR: volume render; BMI: body mass index; AAS: actual arterial subpoint; SL: surface location; PCs: pressurized components; LoA: limits of agreement.

Declarations

Ethics approval and consent to participate:

This study was approved by the Ethics Committee of Daping Hospital (Army Medical Center of PLA) (reference number 2019092) and conducted in adherence with the tenets of the Declaration of Helsinki. Informed consent was waived because patients` private information were hided, and all data were not used for commercial or medical purposes.

Consent for publication:

Not applicable.

Funding:

This study was supported by Clinical Technology Innovation and Cultivation Project of Army Medical University (cx2019js109).

Availability of data and materials:

Please contact the authors for data requests.

Competing interest:

The authors declare that they have no competing interests.

Authors' contributions:

ZHY and ZLY contributed to the study conception and design. LH, ZHY and GY contributed to the acquisition of data and the interpretation of the results. ZHY and GY drafted the manuscript. TH, LY and ZLY critically revised the manuscript. All authors read and approved the final manuscript.

Acknowledgements:

The authors would like to thank professor Wei-guo Zhang, the director of radiology, Daping Hospital for his assistance in this study. Also, we would like to thank Xiao-ying Huang for English language editing.

References

1. Eastridge BJ, Mabry RL, Seguin P, Cantrell J, Blackbourne LH. Death on the battlefield (2001-2011): Implications for the future of combat casualty care. J Trauma Acute Care. 2012;73(6 Suppl 5):431-7.
2. Eastridge BJ, Hardin M, Cantrell J, Oetjen-Gerdes L, Blackbourne LH. Died of wounds on the battlefield: causation and implications for improving combat casualty care. J Trauma. 2011;71 Suppl 1:4-8.
3. Morrison JJ. Noncompressible torso hemorrhage. Crit Care Clin. 2017;33:37-54.
4. Eastridge BJ, Holcomb JB, Shackelford S. Outcomes of traumatic hemorrhagic shock and the epidemiology of preventable death from injury. Transfusion. 2019;59:1423-8.
5. Holcomb JB, Mcmullin NR, Pearse L, Caruso J, Wade CE, Oetjen-Gerdes L, et al. Causes of death in U.S. special operations forces in the global war on terrorism. Ann Surg. 2007;245:986-91.
6. Gaspary MJ, Zarow GJ, Barry MJ, Walchak AC, Conley SP, Roszko PJD. Comparison of three junctional tourniquets using a randomized trial design. Prehosp Emerg Care. 2019;23:187-194.
7. Kheirabadi BS, Terrazas IB, Miranda N, Voelker AN, Grimm R, Kragh JF, et al. Physiological consequences of Abdominal Aortic and Junctional Tourniquet (AAJT) application to control hemorrhage in a swine model. Shock. 2016;46 Suppl 1:160-6.
8. Brännström A, Rocksén D, Hartman J, Nyman N, Gustavsson J, Arborelius UP, et al. Abdominal aortic and junctional tourniquet release after 240 minutes is survivable and associated with small intestine and liver ischemia after porcine class II hemorrhage. J Trauma Acute Care. 2018;85(4):717-24.
9. Kheirabadi BS, Terrazas IB, Miranda N, Voelker AN, Klemcke HG, Brown AW, et al. Long-term consequences of abdominal aortic and junctional tourniquet for hemorrhage control. J Surg Res. 2018;231:99-108.
10. Kheirabadi BS, Terrazas IB, Miranda N, Estep JS, Corona BT, Kragh JF, et al. Long-term effects of combat ready clamp application to control junctional hemorrhage in swine. J Trauma Acute Care.

2014;77(3 Suppl 2):101-8.

11. Magee GA, Fox CJ, Moore EE. Resuscitative endovascular balloon occlusion of the aorta in pelvic ring fractures: The denver health protocol. Injury. 2020;doi:10.1016/j.injury.2020.01.044.
12. Heindl SE, Wiltshire DA, Vahora IS, Tsouklidis N, Khan S. Partial versus complete resuscitative endovascular balloon occlusion of the aorta in exsanguinating trauma patients with non-compressible torso hemorrhage. Cureus. 2020;12(7):e8999.
13. Eliason JL, Derstine BA, Horbal SR, Wang NC, Holcombe SA, Chiu CH, et al. Computed tomography correlation of skeletal landmarks and vascular anatomy in civilian adult trauma patients: Implications for resuscitative endovascular balloon occlusion of the aorta. J Trauma Acute Care. 2019;87(1 Suppl 1):138-45.
14. Douma MJ, Picard C, O'Dochartaigh D, Brindley PG. Proximal external aortic oompression for life-threatening abdominal-pelvic and junctional hemorrhage: an ultrasonographic study in adult volunteers. Prehosp Emerg Care. 2019;23(4):538-42.
15. Okada Y, Narumiya H, Ishi W, Iiduka R. Anatomical landmarks for safely implementing resuscitative balloon occlusion of the aorta (REBOA) in zone 1 without fluoroscopy. Scand J Trauma Resus. 2017;doi:10.1186/s13049-017-0411-z.
16. Morrison JJ, Stannard A, Midwinter MJ, Sharon DJ, Eliason JL, Rasmussen TE. Prospective evaluation of the correlation between torso height and aortic anatomy in respect of a fluoroscopy free aortic balloon occlusion system. Surgery. 2014;155(6):1044-51.
17. Garrett PD, Eckart RE, Bauch TD, Thompson CM, Stajduhar KC. Fluoroscopic localization of the femoral head as a landmark for common femoral artery cannulation. Catheter Cardio Inte. 2010;65(2):205-7.
18. Mirjalili SA, Mcfadden SL, Buckenham T, Stringer MD. A reappraisal of adult abdominal surface anatomy. Clin Anat. 2012;25(7):844–50.
19. Pak N, Patel SG, Hashemi Taheri AP, Hashemi F, Eftekhari Vaghefi R, Naybandi Atashi S, et al. A reappraisal of adult thoracic and abdominal surface anatomy in Iranians in vivo using computed tomography. Clin Anat. 2016;29(2):191-6.
20. Shen XH, Su BY, Liu JJ, Zhang GM, Xue HD, Jin ZY, et al. A reappraisal of adult thoracic and abdominal surface anatomy via CT scan in Chinese population. Clin Anat. 2016;29(2):165-74.
21. Chithriki M, Jaibaji M, Steele R. The anatomical relationship of the aortic bifurcation to the lumbar vertebrae: a MRI study. Surg Radiol Anat. 2002;24(5):308-12.
22. Pirró N, Ciampi D, Champsaur P, Di Marino V. The anatomical relationship of the iliocava junction to the lumbosacral spine and the aortic bifurcation. Surg Radiol Anat. 2005;27(2):137-41.
23. Lakchayapakorn K, Siriprakarn Y. Anatomical variations of the position of the aortic bifurcation, iliocava junction and iliac veins in relation to the lumbar vertebra. J Med Assoc Thai. 2008;91(10):1564-70.
24. Anson BJ, McVay CB. The topographical positions and the mutual relations of the visceral branches of the abdominal aorta. A study of 100 consecutive cadavers. Anat Rec. 1936;67(1):7-15.

25. Nezhat F, Brill AI, Nezhat CH, Nezhat A, Seidman DS, Nezhat C. Laparoscopic appraisal of the anatomic relationship of the umbilicus to the aortic bifurcation. J Am Assoc Gyn Lap. 1998;5(2):135-40.
26. Mulayim B, Gurses C, Karadag B, Sozel YK. The relationship between the umbilicus and the aortic bifurcation in Turkish women: implications for laparoscopic entry. Arch Gynecol Obstet. 2017;296(6):1175-80.
27. Hurd WW, Bude RO, DeLancey JOL, Pearl ML. The relationship of the umbilicus to the aortic bifurcation: Implications for laparoscopic technique. Obstet Gynecol. 1992;80(1):48-51.
28. Attwell L, Rosen S, Upadhyay B, Gogalniceanu P. The umbilicus: a reliable surface landmark for the aortic bifurcation? Surg Radiol Anat. 2015;37(10):1239-42.
29. Jeong JY, Kim YR, Kim JY, Jee BC, Kim SH. Vertical distance between umbilicus to aortic bifurcation on coronal view in Korean women. Obstet Gynecol Sci. 2014;57(1):44-9.
30. Kuk JL, Saunders TJ, Davidson LE, Ross R. Age-related changes in total and regional fat distribution. Ageing Res Rev. 2009;8(4):339-48.
31. Larsson L, Grimby G, Karlsson J. Muscle strength and speed of movement in relation to age and muscle morphology. J Appl Physiol Respir Environ Exerc Physiol. 1979;46(3):451-6.
32. Ota M, Ikezoe T, Kato T, Tateuchi H, Ichihashi N. Age-related changes in muscle thickness and echo intensity of trunk muscles in healthy women: comparison of 20–60s age groups. Eur J Appl Physiol. 2020;120(8):1805-14.
33. Stannard A, Morrison JJ, Sharon DJ, Eliason JL, Rasmussen TE. Morphometric analysis of torso arterial anatomy with implications for resuscitative aortic occlusion. J Trauma Acute Care Surg. 2013;75(2 Suppl 2):169-72.
34. Taylor DM, Coleman M, Parker PJ. The evaluation of an abdominal aortic tourniquet for the control of pelvic and lower limb hemorrhage. Mil Med. 2013;178(11):1196-201.
35. Lyon M, Shiver SA, Greenfield EM, Reynolds BZ, Lerner EB, Wedmore IS, et al. Use of a novel abdominal aortic tourniquet to reduce or eliminate flow in the common femoral artery in human subjects. J Trauma Acute Care Surg. 2012;73(2 Suppl 1):103-05.
36. Kragh JF KR, Cap AP, et al. Performance of junctional tourniquets in normal human volunteers. Prehosp Emerg Care. 2015;19:391-8.
37. Bland JM, Altman DG. Statistical methods for assessing agreement between two methods of clinical measurement. Lancet. 1986;doi:10.1016/S0140-6736(86)90837-8.
38. Tibbits EM, Hoareau GL, Simon MA, Davidson AJ, DeSoucy ES, Faulconer ER, et al. Location is everything: the hemodynamic effects of REBOA in zone 1 versus zone 3 of the aorta. J Trauma Acute Care Surg. 2018;85(1):101-7.
39. Van Oostendorp SE, Tan ECTH, Geeraedts LMG. pre-hospital control of life-threatening truncal and junctional haemorrhage is the ultimate challenge in optimizing trauma care; a review of treatment options and their applicability in the civilian trauma setting. Scand J Trauma Resusc Emerg Med. 2016;doi:10.1186/s13049-016-0301-9.

40. Morrison JJ, Yapp LZ, Beattie A, Devlin E, Jansen JO. The epidemiology of Scottish trauma: a comparison of pre-hospital and in-hospital deaths, 2000 to 2011. Surg-J Royal Coll Surg E. 2016;14(1):1-6.
41. Rhee P, Joseph B, Pandit V, Aziz H, Vercruysse G, Kulvatunyou N, et al. Increasing trauma deaths in the United States. Ann Surg. 2014;260(1):13-21.
42. Teixeira PGR, Inaba K, Hadjizacharia P, Brown C, Salim A, Rhee P, et al. Preventable or potentially preventable mortality at a mature trauma center. J Trauma. 2007;63(6):1338-46.
43. The Lancet. COVID-19: remaking the social contract. The Lancet. 2020;395(10234):1401.
44. Jin YH, Huang Q, Wang YY, Zeng XT, Luo LS, Pan ZY, et al. Perceived infection transmission routes, infection control practices, psychosocial changes, and management of COVID-19 infected healthcare workers in a tertiary acute care hospital in Wuhan: a cross-sectional survey. Mil Med Res. 2020;doi: 10.1186/s40779-020-00254-8.
45. Zheng LC, Wang X, Zhou CC, Liu Q, Li S, Sun Q, et al. Analysis of the infection status of the health care workers in Wuhan during the COVID-19 outbreak: A cross-sectional study. Clin Infect Dis. 2020;doi:10.1093/cid/ciaa588.

Figures

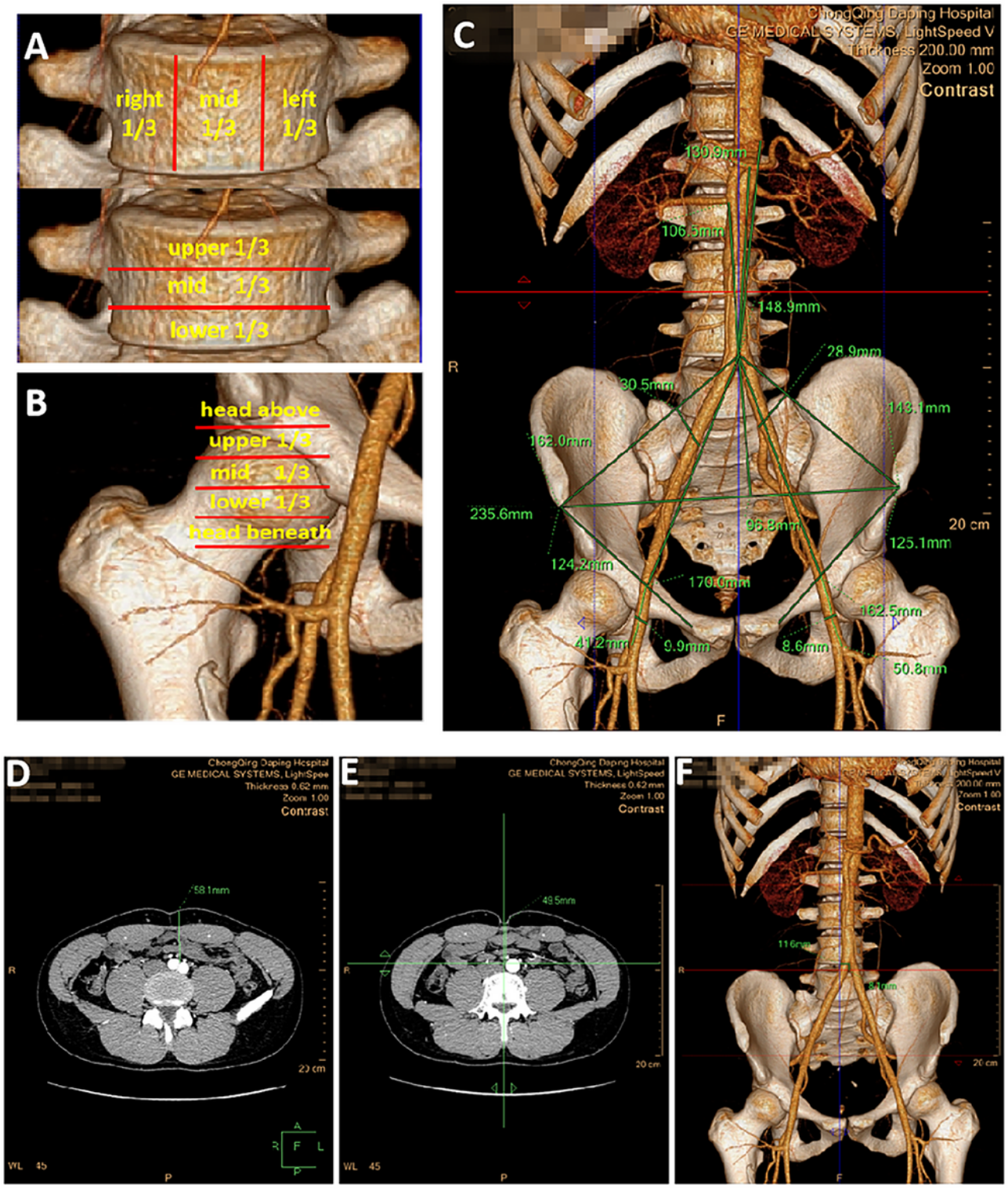

Figure 1

Measurements via contrast-enhanced CT imaging. A: Horizontal and vertical trisections of the vertebrae. B: Quintiles of the femoral head. C: The lengths of arteries and landmarks were measured through VR images, and the lengths of the CET-AB, AB-left ASIS and left CFA were 148.9 mm, 143.1 mm and 50.8 mm, respectively. D: The vertical distance of the AB-body surface was 58.1 mm. E: The vertical distance of the umbilicus-AB was 49.5 mm. F: The umbilical subpoint is located in the third quadrant (-11.6 mm,

8.1 mm), with AB as the origin of the coordinate axis. VR: volume render, CET: celiac trunk, AB: aortic bifurcation, ASIS: anterior superior iliac spine, CFA: common femoral artery

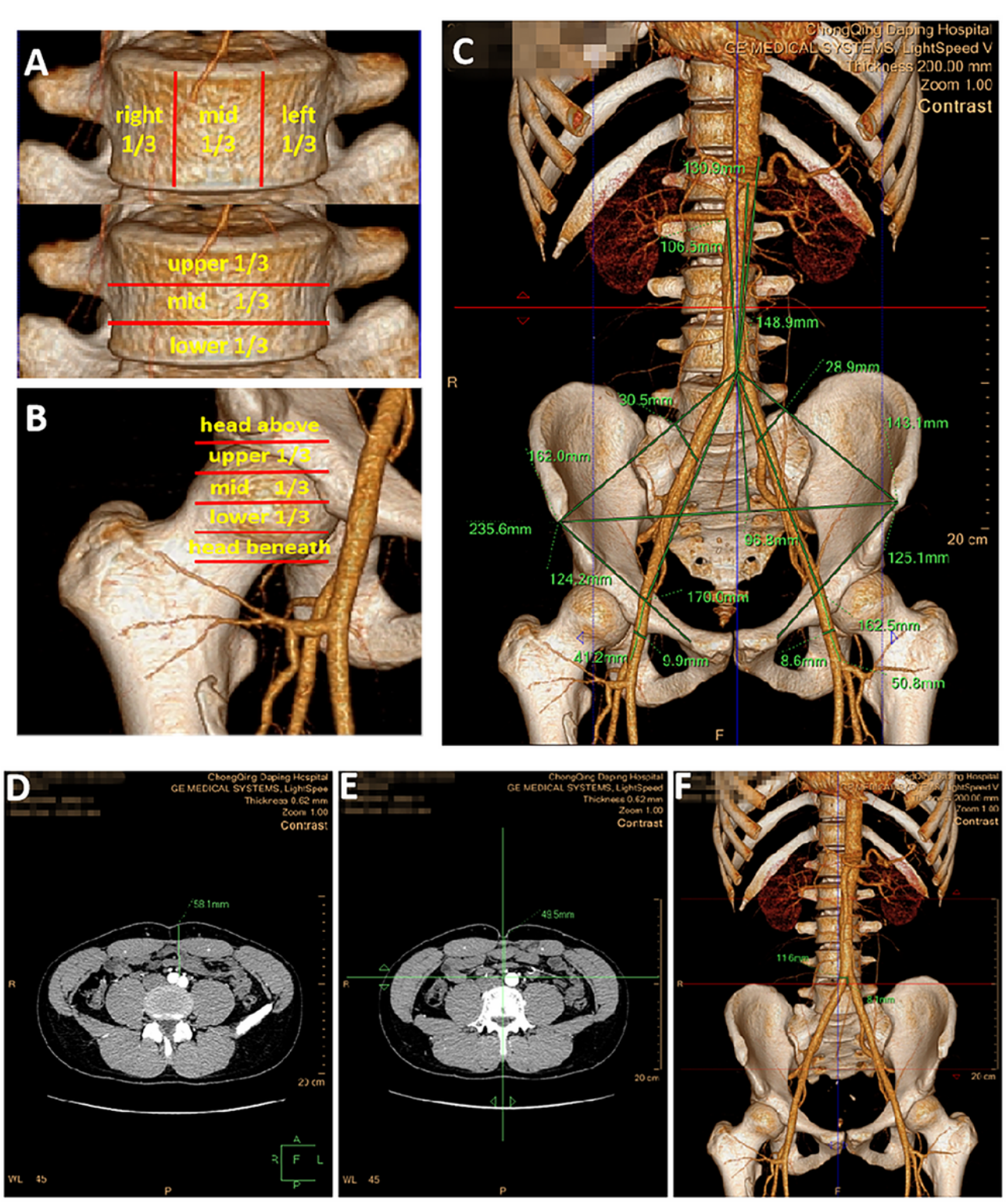

Figure 1

Measurements via contrast-enhanced CT imaging. A: Horizontal and vertical trisections of the vertebrae. B: Quintiles of the femoral head. C: The lengths of arteries and landmarks were measured through VR images, and the lengths of the CET-AB, AB-left ASIS and left CFA were 148.9 mm, 143.1 mm and 50.8

mm, respectively. D: The vertical distance of the AB-body surface was 58.1 mm. E: The vertical distance of the umbilicus-AB was 49.5 mm. F: The umbilical subpoint is located in the third quadrant (-11.6 mm, 8.1 mm), with AB as the origin of the coordinate axis. VR: volume render, CET: celiac trunk, AB: aortic bifurcation, ASIS: anterior superior iliac spine, CFA: common femoral artery

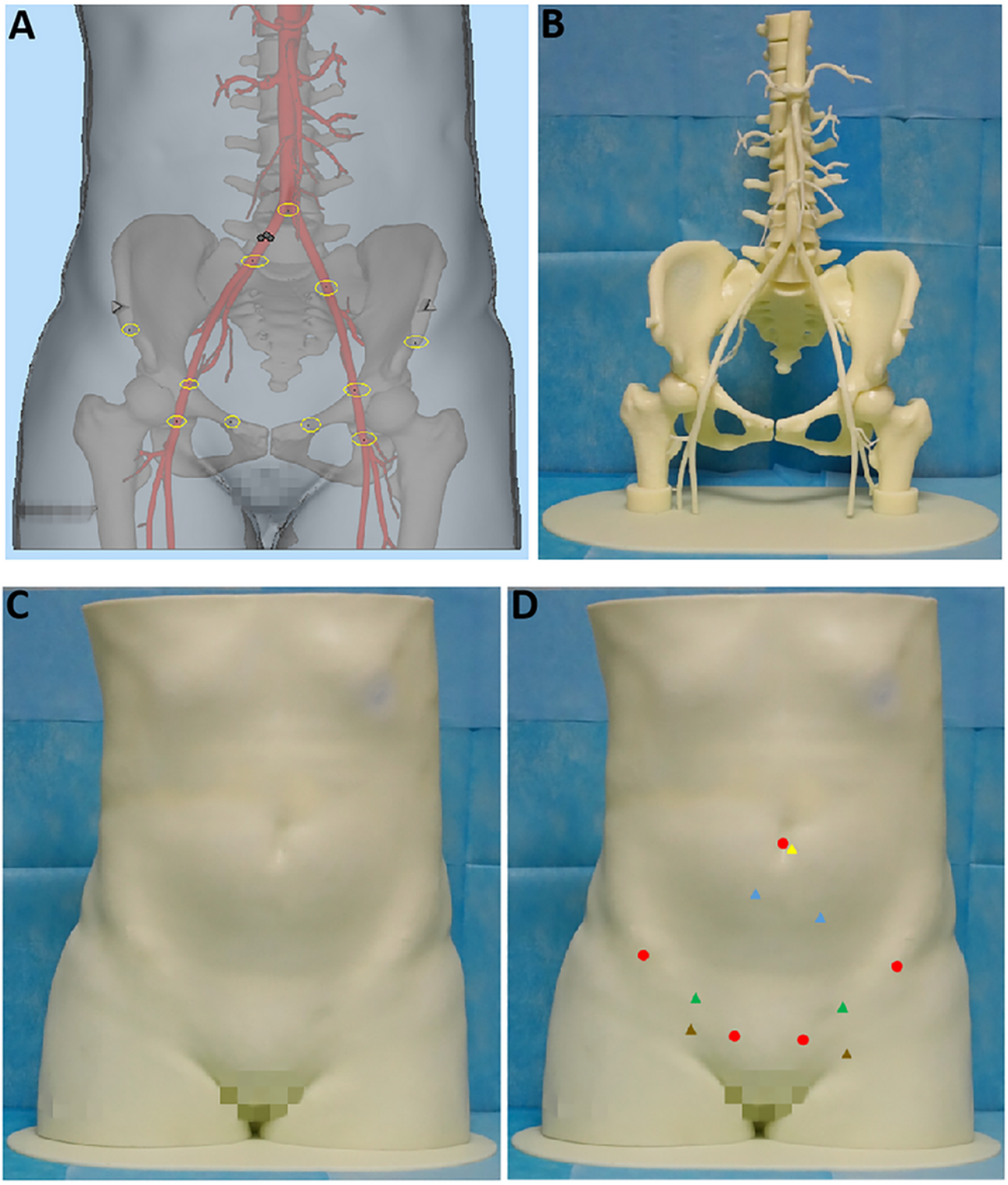

Figure 2

A full-size 3D-printed model of a female patient. A: Projection points of EHCD-targeted arteries, the ASIS and the PT were identified during image reconstruction. B: EHCD-targeted arteries, the pelvic ring and the spine were completely printed. C: Body surface of the model. D: Red dots represent the projection points of the umbilicus, ASIS and PT, and the yellow, blue, green and brown triangles represent the actual surface locations of the AB and CIA/EIA/CFA termini, respectively. EHCDs: external hemorrhage control devices, ASIS: anterior superior iliac spine, PT: pubic tubercle, AB: aortic bifurcation, CIA: common iliac artery, EIA: external iliac artery, CFA: common femoral artery

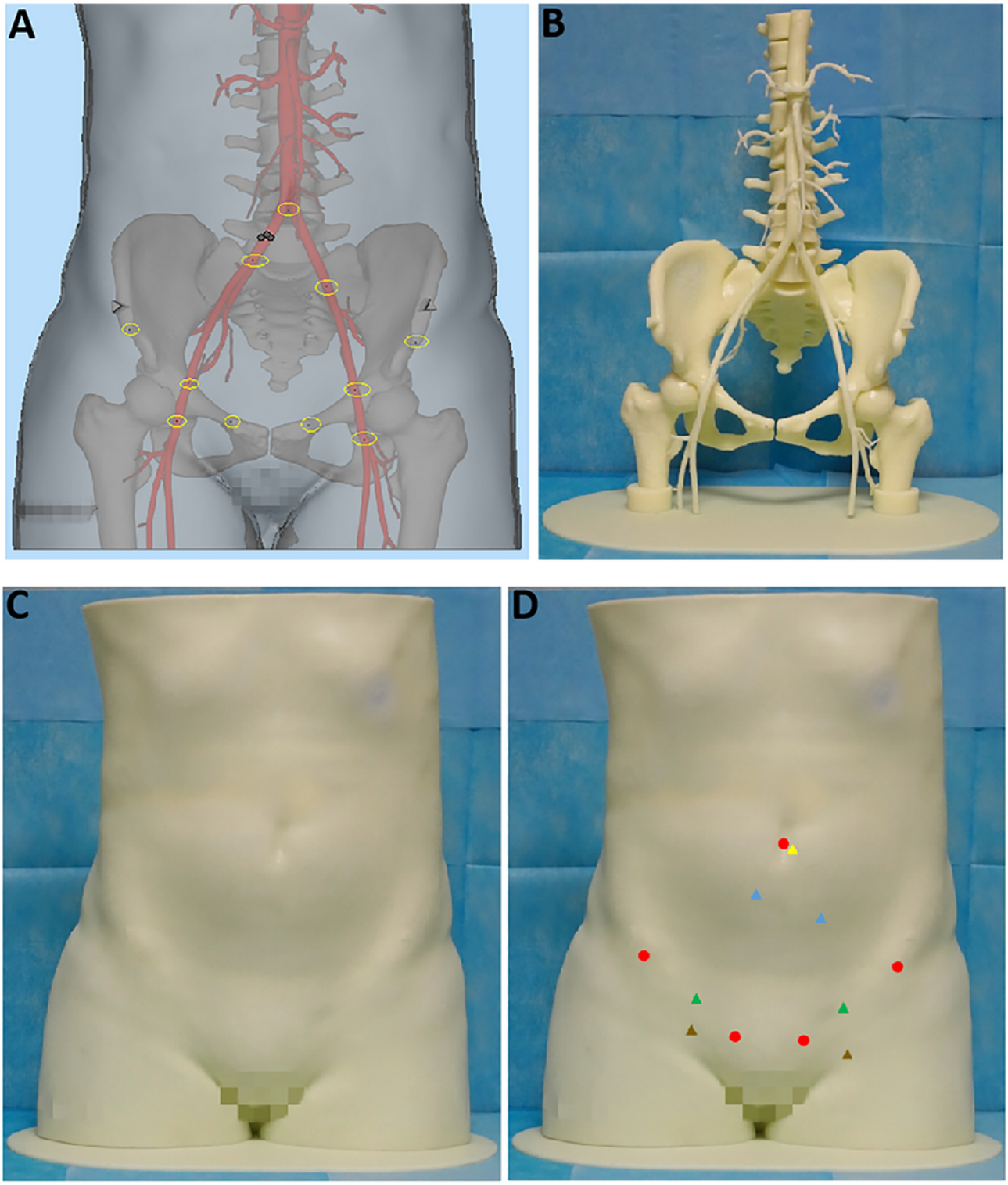

Figure 2

A full-size 3D-printed model of a female patient. A: Projection points of EHCD-targeted arteries, the ASIS and the PT were identified during image reconstruction. B: EHCD-targeted arteries, the pelvic ring and the spine were completely printed. C: Body surface of the model. D: Red dots represent the projection points of the umbilicus, ASIS and PT, and the yellow, blue, green and brown triangles represent the actual surface locations of the AB and CIA/EIA/CFA termini, respectively. EHCDs: external hemorrhage control devices, ASIS: anterior superior iliac spine, PT: pubic tubercle, AB: aortic bifurcation, CIA: common iliac artery, EIA: external iliac artery, CFA: common femoral artery

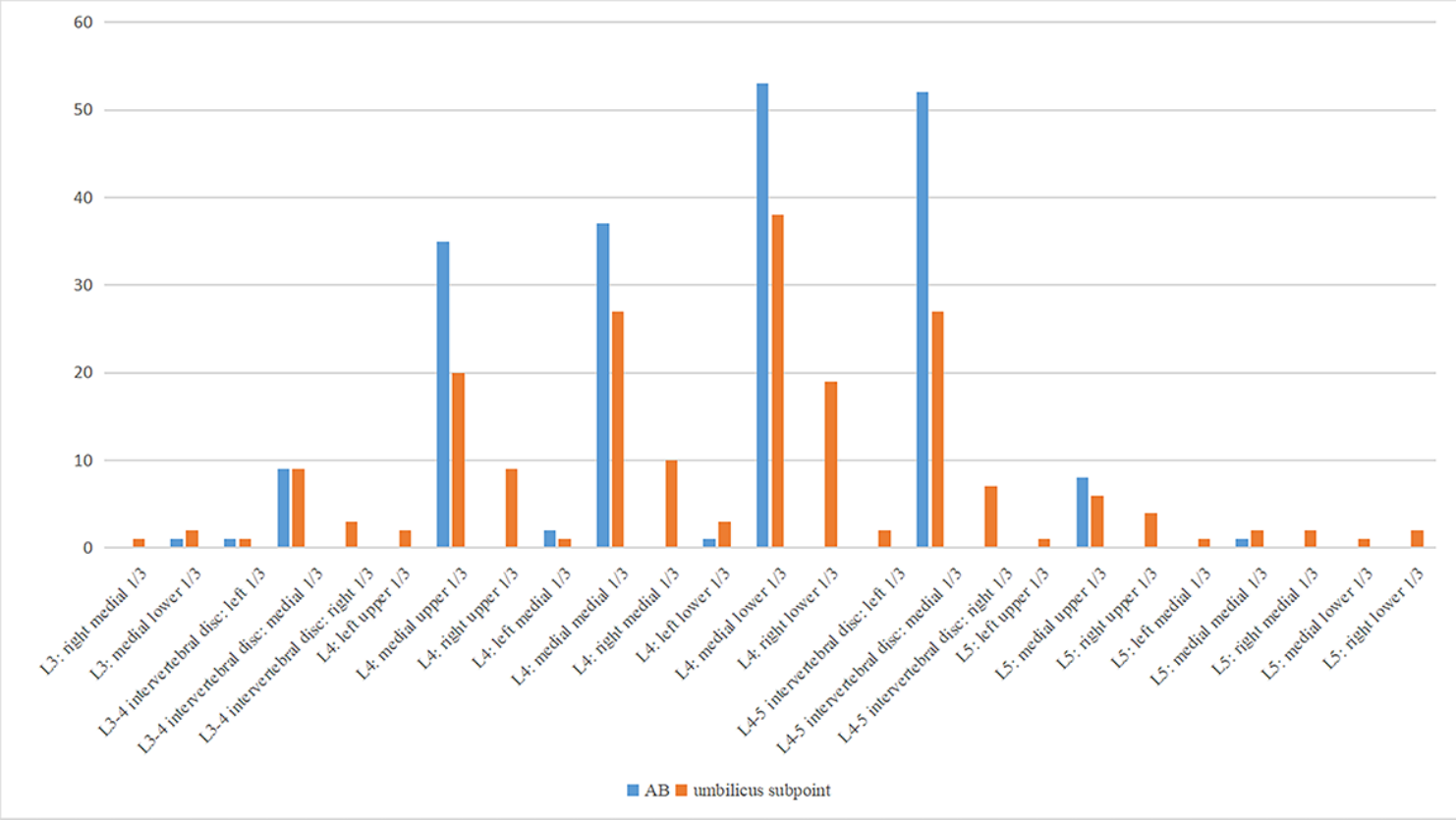

Figure 3

Distribution of AB and umbilical subpoints referenced by vertebrae. AB: aortic bifurcation

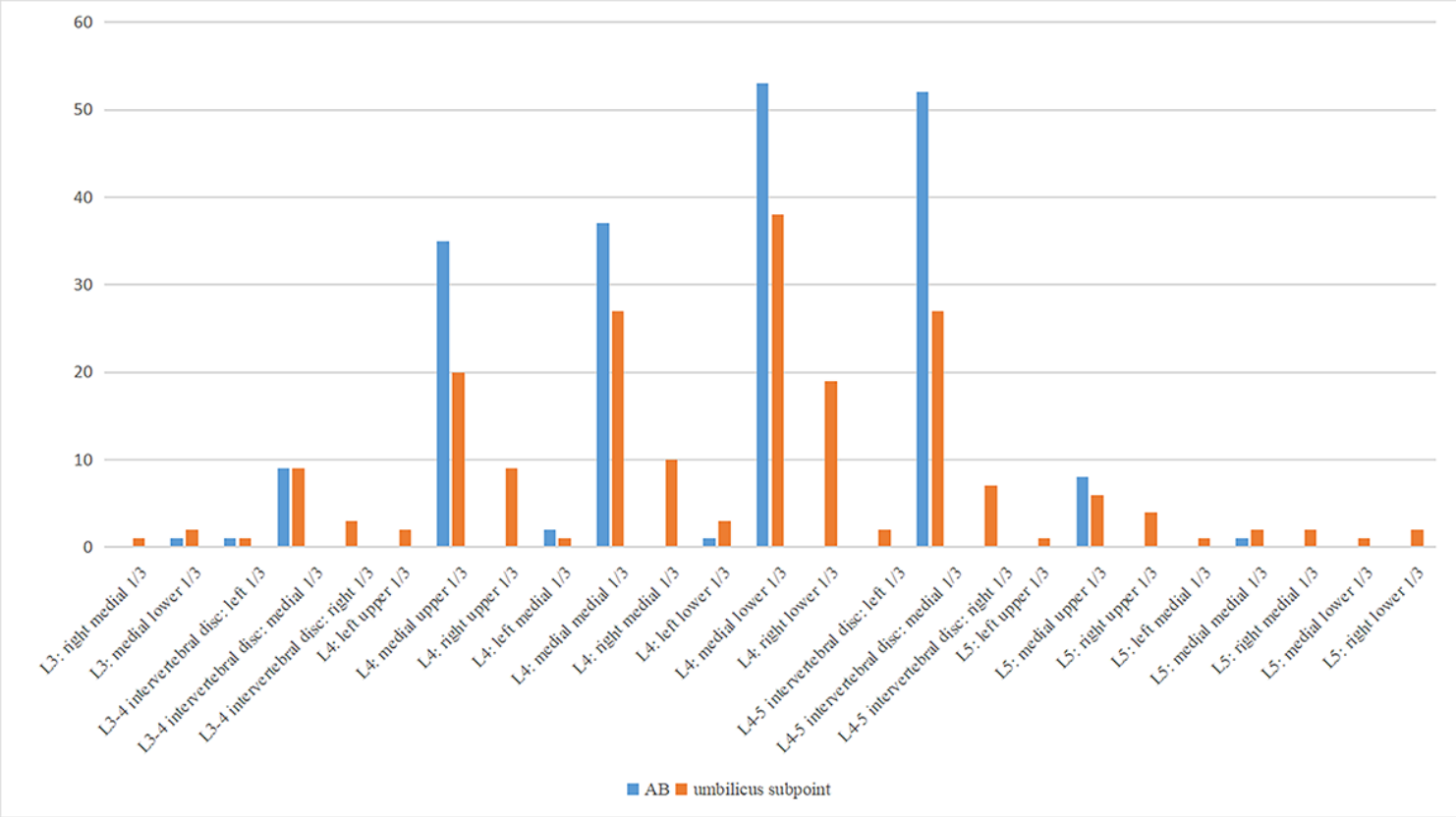

Figure 3

Distribution of AB and umbilical subpoints referenced by vertebrae. AB: aortic bifurcation

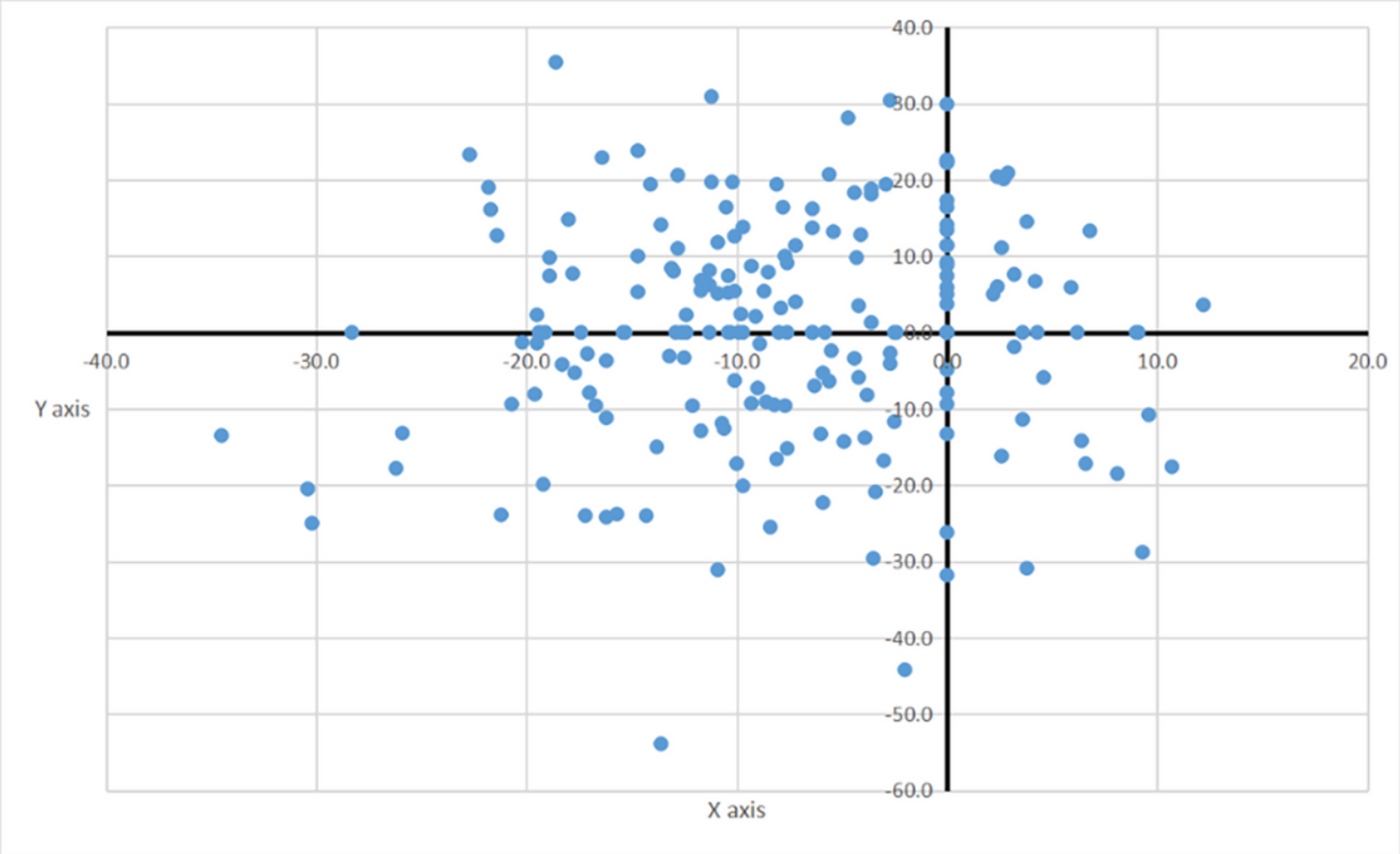

Figure 4

Distribution of umbilicus subpoints. The umbilicus was mainly distributed in the second and third quadrants (61.5%), taking the AB as the origin of the coordinates. AB: aortic bifurcation

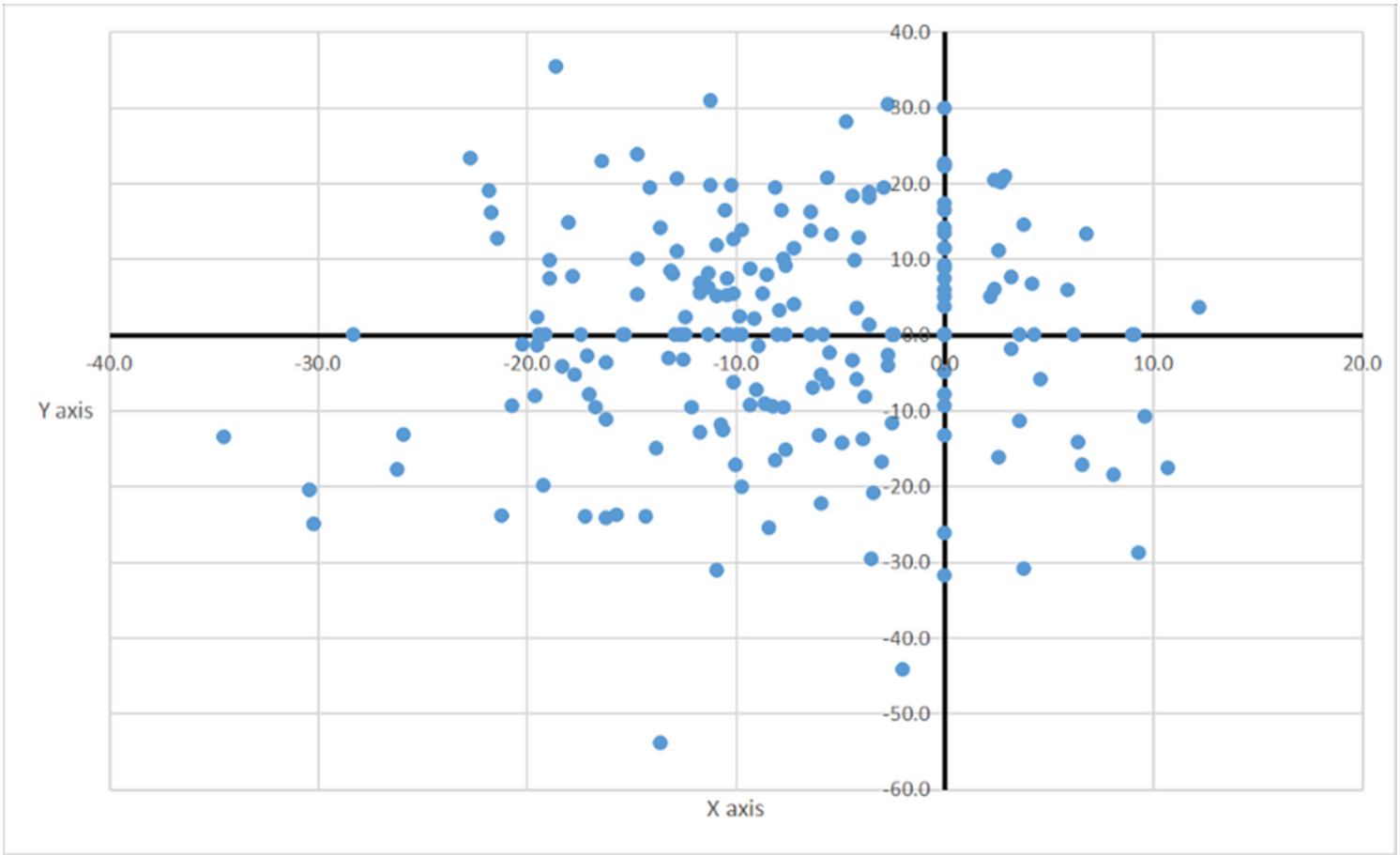

Figure 4

Distribution of umbilicus subpoints. The umbilicus was mainly distributed in the second and third quadrants (61.5%), taking the AB as the origin of the coordinates. AB: aortic bifurcation

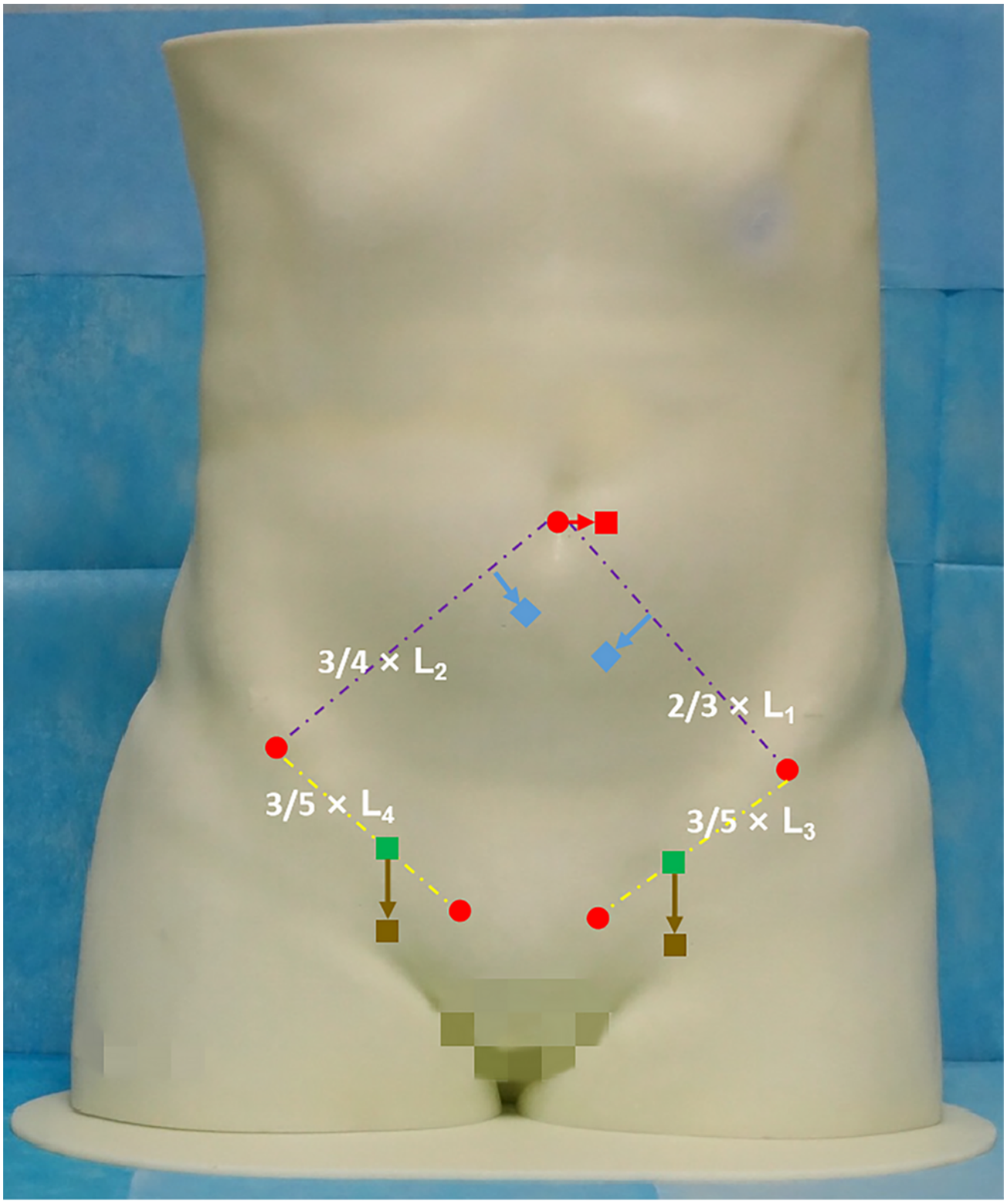

Figure 5

Surface localization of EHCD-related arteries. Red, blue, green and brown squares represent the AB and CIA/EIA/CFA termini, respectively. The red arrow indicates 1 finger breadth left to the umbilicus (red circle), the blue arrow indicates 1 finger breadth parallel to the umbilicus-ASIS, and the brown arrow demonstrates 2 finger breadths (female) or 3 fingers (male) vertically downward from the EIA terminus. L1 and L2: length of umbilicus-ASIS, L3 and L4: length of ASIS-homolateral PT. EHCDs: external

hemorrhage control devices, AB: aortic bifurcation, ASIS: anterior superior iliac spine, PT: pubic tubercle, CIA: common iliac artery, EIA: external iliac artery, CFA: common femoral artery

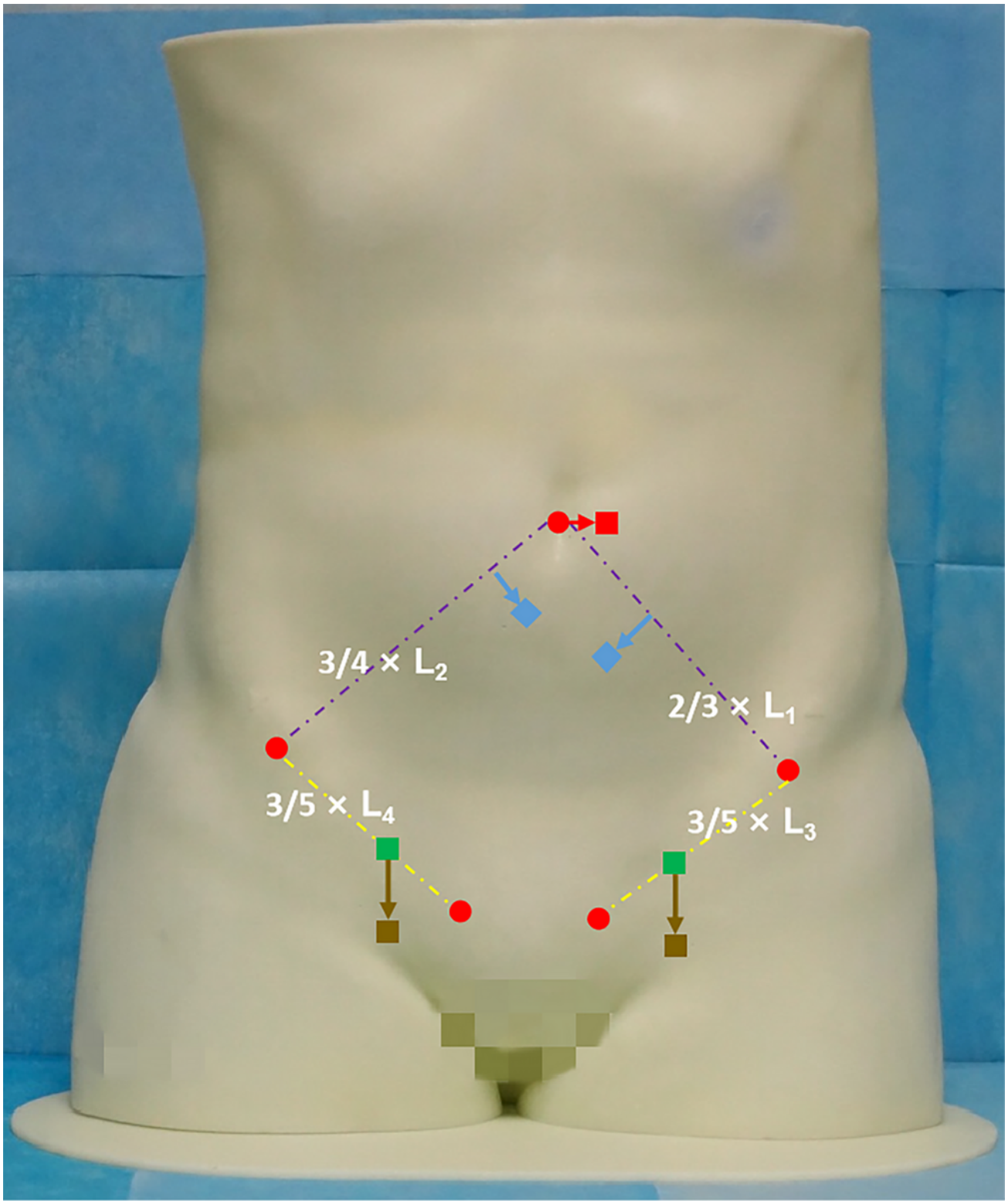

Figure 5

Surface localization of EHCD-related arteries. Red, blue, green and brown squares represent the AB and CIA/EIA/CFA termini, respectively. The red arrow indicates 1 finger breadth left to the umbilicus (red circle), the blue arrow indicates 1 finger breadth parallel to the umbilicus-ASIS, and the brown arrow

demonstrates 2 finger breadths (female) or 3 fingers (male) vertically downward from the EIA terminus. L1 and L2: length of umbilicus-ASIS, L3 and L4: length of ASIS-homolateral PT. EHCDs: external hemorrhage control devices, AB: aortic bifurcation, ASIS: anterior superior iliac spine, PT: pubic tubercle, CIA: common iliac artery, EIA: external iliac artery, CFA: common femoral artery

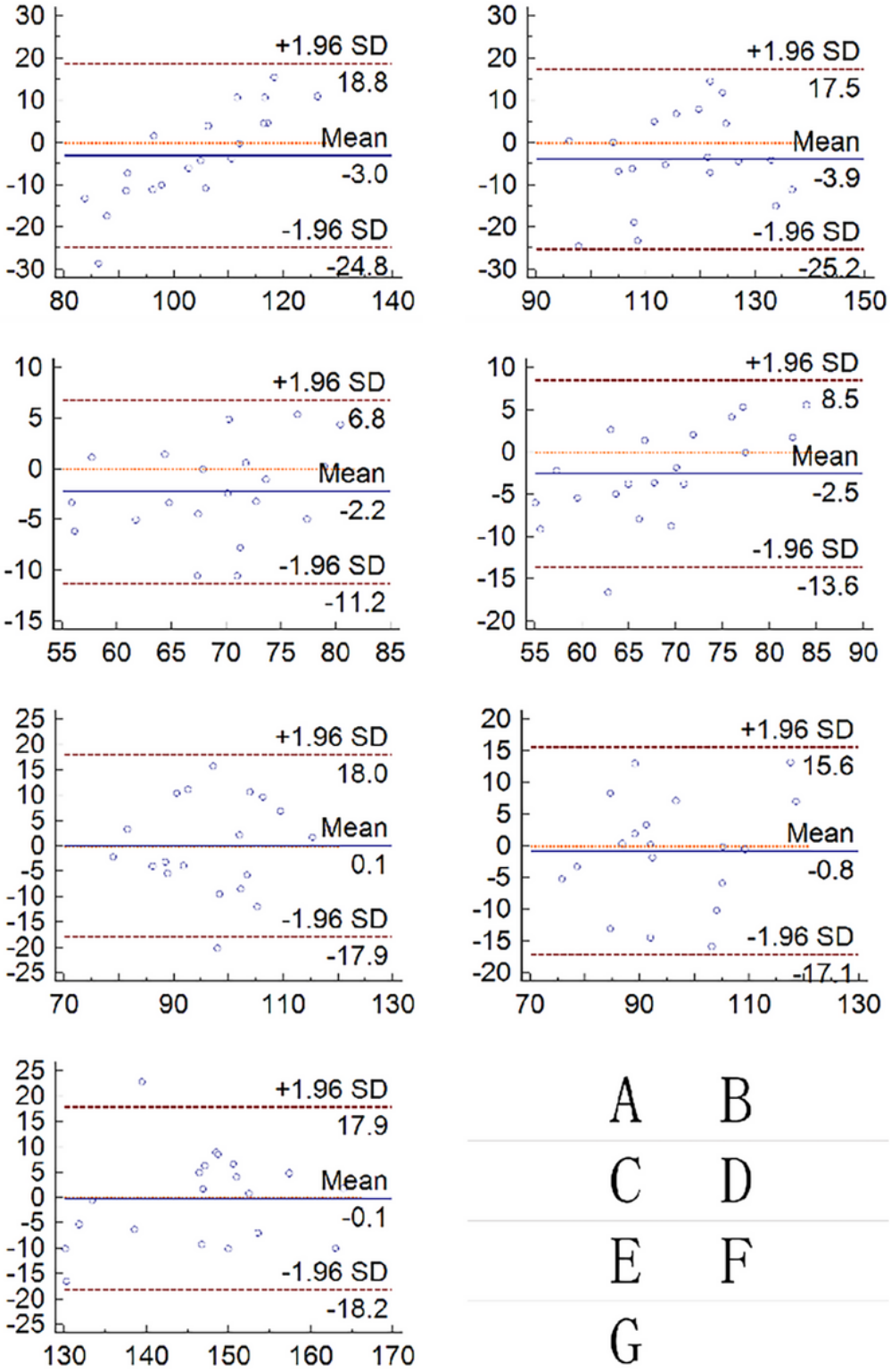

Figure 6

Bland-Altman consistency analysis between the AAS and the SL to the corresponding ASIS. A and B: Left and right CIA terminus and SLs. C and D: EIA termini and SLs. E and F: CFA termini and SLs, G: AB and SL. All graphs met the criteria that at least 95% (19/20) of dots were situated within the limits of agreement (LoA). The mean distance difference of the AAS-SL ranged from -0.1 mm (AB) to 3.9 mm (right CIA terminus), while the relative error ranged from 5.0% (AB) to 9.1% (left CIA terminus). AAS: actual arterial subpoint, SL: surface location, AB: aortic bifurcation, CIA: common iliac artery, EIA: external iliac artery, CFA: common femoral artery, ASIS: anterior superior iliac spine

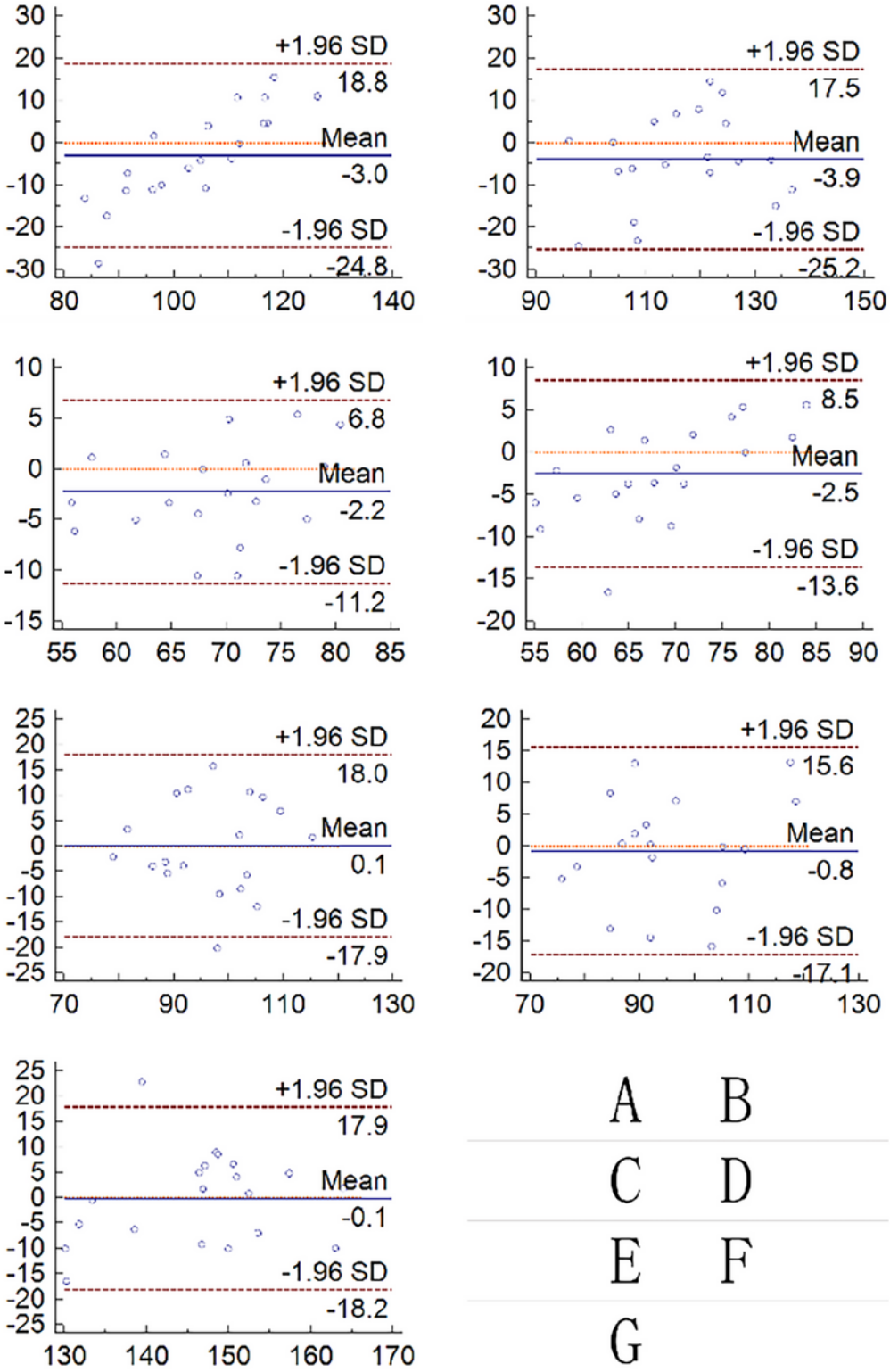

Figure 6

Bland-Altman consistency analysis between the AAS and the SL to the corresponding ASIS. A and B: Left and right CIA terminus and SLs. C and D: EIA termini and SLs. E and F: CFA termini and SLs, G: AB and SL. All graphs met the criteria that at least 95% (19/20) of dots were situated within the limits of agreement (LoA). The mean distance difference of the AAS-SL ranged from -0.1 mm (AB) to 3.9 mm (right CIA terminus), while the relative error ranged from 5.0% (AB) to 9.1% (left CIA terminus). AAS: actual arterial subpoint, SL: surface location, AB: aortic bifurcation, CIA: common iliac artery, EIA: external iliac artery, CFA: common femoral artery, ASIS: anterior superior iliac spine